ChemComm

ROYAL SOCIETY OF CHEMISTRY

COMMUNICATION

View Article Online
View Journal | View Issue

Check for updates

Cite this: *Chem. Commun.*, 2025, **61**, 8919

Received 8th January 2025,
Accepted 3rd May 2025

DOI: 10.1039/d5cc00117j

rsc.li/chemcomm

A mixed metallic and mixed valence $Mo^{V}_{4}V^{IV}_{2}V^{III}_{2}$ complex as an electron transfer photo-catalyst for the hydrogen evolution reaction†

Kalyankumar S. Morla,‡[a] Dewendra Thakre,‡[a] Adarsh K. Mourya,[a] Piyush Singh,[a] Harsha S. Karnamkkott,[b] Subuhan Ahamed,[b] Subham Sahoo,[c] Ishita Bhattacharya,[a] Siddhartha Banerjee,[a] Debajit Sarma,[c] Kartik Chandra Mondal,*[b] Sujit Kumar Ghosh,*[a] Atul V. Wankhade*[a] and Abhishek Banerjee*[a]

Ligand-directed structure modulation is observed during the synthesis of mixed-metallic vanado-molybdate complexes functionalized with pyridinyl diphosphonate ligand(s). The structural assembly is determined by the location of the nitrogen-atom at the aromatic ring of the pyridinyl-ligands, forming either a tetranuclear mixed-valence V(III/IV)-containing complex (1) having a butterfly-like structure, or a monocentric S-shaped complex (2) containing an octahedral V(III). Photocatalytic hydrogen evolution from water (HER) studies show higher catalytic activity by complex 1, as compared with complex 2, attributed to the delocalization of spin densities between V(III) and V(IV) in 1. The transfer of electrons from vanadium(III and IV) mixed-valence complex 1 to H^+ is more facile than from the vanadium(III) homo-valent complex 2. A dominant reductive quenching mechanism has been further established by detailed photophysical studies of 1.

Polyoxometalates (POMs) have shown great potential and versatility to act as efficient redox catalysts.[1,2] Well-defined structures, and a variety of metal atoms and cluster shapes in POMs, allow for precise manipulation of their electronic properties, enhancing activity and stability, as well as customization of their performances.[3] The inherent redox activity of POMs enables easy electron transfer in water oxidation or reduction.[4,5] Exploration of POMs as photocatalysts for the hydrogen evolution reaction (HER) from water[6] has mostly been with oxo-tungstates,[7,8] or oxo-molybdates.[9] Hill and co-workers have extensively reported 3d-transition metal clusters embedded within tungstates.[7] Other research groups have also reported on the photocatalytic HER with lacunary tungstate derivatives containing 3d-metal clusters.[10–15] However, the only report of an oxo-vanadate complex as a catalyst for photochemical water splitting is from Campagna and co-workers, *viz.* the mixed-valence anion $[(V^{IV}_{5}V^{V})O_7(OCH_3)_{12}]^-$.[16]

To further investigate the photocatalytic HER with POMs, we have explored the mixed-metallic oxo-vanado-molybdate system. Vanadium's ability to exist in multiple oxidation states and coordination environments makes poly-oxovanadates (POVs), particularly mixed-valent oxo-vanadates, excellent candidates as redox catalysts,[17,18] and energy storage materials.[19,20] However, our initial studies on the photocatalytic HER with oxo-vanadates were not promising.[21] Subsequently, our studies with the mixed-metal oxo-vanado-molybdate complexes, presented here, have yielded promising results. Herein, we report on the synthesis, characterization and photocatalytic HER studies of two Mo-V complexes with diphosphonate functionalized ligands, *viz.* $H_{10}[(Mo^{V}_{2}O_4)_2(V^{III}_{2}O_2)(V^{IV}O)_2\{O_3P–C(O)(CH_2\text{-}2\text{-}C_5NH_4)–PO_3\}_4]\cdot 25H_2O$ (**1a**) having a mixed valence $V^{IV}_{2}V^{III}{}_{2}$ unit at the centre and an octahedral V^{III}-containing complex $H_5[(Mo^{VI}_{2}O_5)_2(V^{III}O_2)\{O_3P–C(O)(CH_2\text{-}4\text{-}C_5NH_5)–PO_3\}_2]\cdot 16H_2O$ (**2a**).

Both compounds were synthesized using a one-pot reaction of $[Mo^{V}_{2}O_4(H_2O)_6]^{2+}$ with $NaVO_3$ and the respective diphosphate ligand, in aqueous solution (Scheme 1).

The structures of the complexes were determined using single crystal X-ray diffraction analyses, showing that both **1a** and **2a** crystallize in the monoclinic crystal system with space groups $C2/m$ and $P2_1/n$, respectively, having a centre of symmetry in them [Table S1, ESI†]. Due to the overall symmetry of the polyanionic assemblies, $[(Mo^{V}_{2}O_4)_2(V^{III}_{2}O_2)(V^{IV}O)_2\{O_3P–C(O)(CH_2\text{-}2\text{-}C_5H_4N)–PO_3\}_4]^{10-}$ (**1**) and $[(Mo^{VI}_{2}O_5)_2(V^{III}O_2)\{O_3P–C(O)(CH_2\text{-}4\text{-}C_5NH_5)–PO_3\}_2]^{5-}$ (**2**), in both these compounds, many atom(s) in the asymmetric unit(s) are observed to be located in special positions. The oxidation states of the metal atoms, including the mixed-valent vanadium in **1a**, were determined

---

[a] *Department of Chemistry, Visvesvaraya National Institute of Technology, Nagpur–440010, India. E-mail: abhishekbanerjee@chm.vnit.ac.in*
[b] *Department of Chemistry, Indian Institute of Technology Madras, Chennai – 600036, India*
[c] *Department of Chemistry, Indian Institute of Technology Patna, Patna – 801103, India*

† Electronic supplementary information (ESI) available. CCDC 2369137 and 2442530. For ESI and crystallographic data in CIF or other electronic format see DOI: **https://doi.org/10.1039/d5cc00117j**

‡ Both contributed equally to this work.

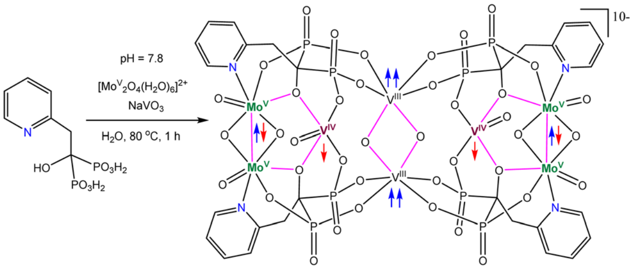

Scheme 1 Synthesis of diphosphonate functionalized mixed metallic vanado-molybdates, forming the mixed valence $Mo^V_4V^{IV}_2V^{III}_2$ (**1**).

through bond-valence sum (BVS) calculations, spectroscopy, and magnetic studies.

For polyanion **1**, BVS calculations assign an oxidation state of +5 to molybdenum and +3/+ 4 to the vanadium atoms [Table S2, ESI†]. Polyanion **1** exhibits a butterfly-like structure with a central $\{V^{III}_2O_2\}$ dimer, where vanadium(III) adopts a distorted octahedral geometry. This unit is capped by two $\{V^{IV}O\}$ units in a distorted square-pyramidal geometry and two $\{Mo^V_2O_4\}$ units, connected *via* fully deprotonated diphosphonate ligands. The octanuclear core forms a mixed-valent heterometallic species, $[(Mo^V_2O_5)_2(V^{IV}O)_2(V^{III}_2O_2)]$ [Fig. 1]. Each molybdenum centre is coordinated by a terminal oxo group and a rare molybdenum-nitrogen bond,[22] enabled by the *ortho*-positioned nitrogen atoms within the diphosphonate linkers.

For polyanion **2**, the oxidation state of molybdenum and vanadium atoms was determined to be +6 and +3, respectively [for BVS calculations, see Table S3, ESI†]. The polyanion structure resembles an S-shaped assembly of two $\{Mo^{VI}_2O_5\}$ units connected to each other by the central $\{V^{III}O_2\}$ unit and capped by the diphosphonate ligand(s) on either side [Fig. S1, ESI†]. The packing arrangement for compounds **1a** and **2a** is shown in Fig. S2 and S3 in the ESI.† PXRD studies confirm the phase purity for compounds **1a** and **2a** [Fig. S4 and S5, ESI†]. The detailed structural analysis reveals the influence of the ligand towards the final assembly of the polyanion, *viz.* ligand directing structure modulation. The proximity of the nitrogen to the molybdenum in **1** makes the formation of the Mo–N bond feasible in **1** but not in **2**. Such a behaviour has hitherto not been observed in polyoxometalate chemistry before.

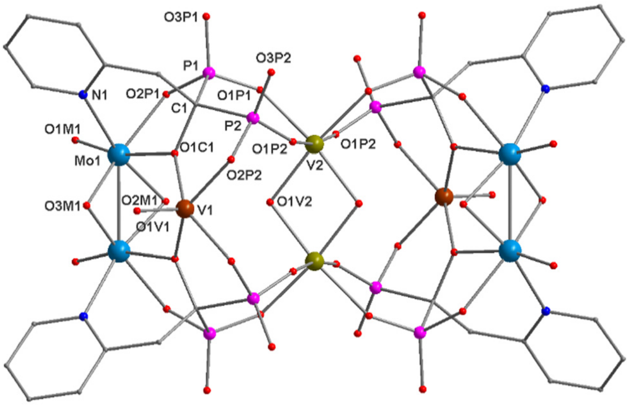

Fig. 1 Ball and stick representation of polyanion $[(Mo^V_2O_4)_2(V^{III}_2O_2)(V^{IV}O)_2]\{O_3P{-}C(O)(CH_2\text{-}2\text{-}C_5H_4N){-}PO_3\}^{10-}$ (**1**).

Time dependent UV-visible spectroscopy confirms extended solution stability of the compounds [Fig. S7, ESI†]. From UV-DRS studies the energy bandgap for **1a** and **2a** was determined to be 1.55 and 1.78 eV, respectively [Fig. S8, ESI†]. The lower energy gap in **1a** corroborates the high nuclear metallic centres over **2a**, containing a single addenda metal atom. The vanadium XPS spectrum of **1a** reveals four overlapping bands, with binding energies at 523.4 and 515.9 eV indicating V^{4+} (V $2p_{3/2}$ and V $2p_{1/2}$), and 524.1 and 517 eV corresponding to V^{3+} (V $2p_{3/2}$ and V $2p_{5/2}$), consistent with literature values [Fig. S9, ESI†].[23,24] The presence of shoulder peaks is indicative of the mixed-valent nature of vanadium present within **1a**. The XPS spectra of **2a** was better resolved, ostensibly due to the presence of homo-valent vanadium, with V 2p peaks at 522.8 eV and 516.7 eV, corresponding to V $2p_{1/2}$ and V $2p_{3/2}$, respectively, affirming a +3-oxidation state for vanadium.[20,24,25]

The solid-state EPR spectra of both the compounds showed hyperfine splitting between 200–500 mT, centred at 341 mT at rt and at 77 K. The X-band EPR spectrum of **1a** at 300 K exhibited anisotropic signals with rhombic symmetry [Fig. S10(a), ESI†], attributed to interactions between a free electron (spin = 1/2) and vanadium nucleus ($I = 7/2$; ^{51}V).[26] Cooling the solid sample improved the signal intensity and resolution without significant changes to the hyperfine structures, indicating similar electron delocalization across vanadium centres under both conditions [Fig. 2 left]. At 77 K, slower electron hopping resulted in improved amplitude. The simulated spectrum of **1a** yielded $g_x = 2.00986$, $g_y = 2.00998$, and $g_z = 2.04998$ using EasySpin.[27] For **2a**, multiple hyperfine lines were also observed and simulated with V(III) parameters ($g_x = 1.9907$, $g_y = 1.99908$, $g_z = 2.03178$) [Fig. S10(b), ESI†].[20]

Magnetic studies on **1a** provided the definitive evidence toward the presence of mixed-valence in V(III and IV). Complex **1a** contains two isolated V(IV) paramagnetic sites ($S = 1/2$) at the wing position(s) of a tetranuclear butterfly core, linked *via* a central $\{V^{III}_2O_2\}$ unit (body position, $S = 1$) [Fig. 3]. Variable-temperature magnetic susceptibility measurements (2–300 K, 0.1 T) show that the χT product of **1a** is 2.42 cm^3 K mol^{-1} at 300 K, close to the value for non-interacting two V(III) (χT = 2.02 cm^3 K mol^{-1}) and two V(IV) (χT = 0.75 cm^3 K mol^{-1}) ions. The χT product slightly increases to 2.46 cm^3 K mol^{-1} at 150 K,

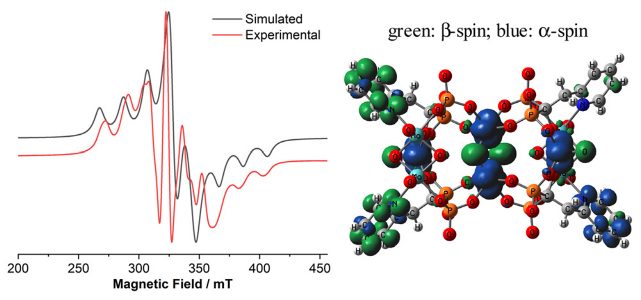

Fig. 2 X-band EPR spectra of **1a** (left) and Mulliken spin densities of **1** (right) at $S = 1$ computed at the B3LYP-D3(BJ)/Def2-SVP level of theory.

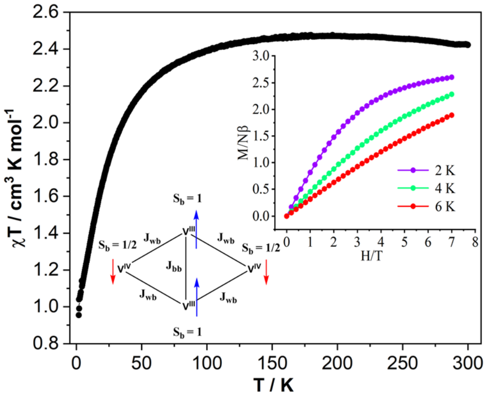

Fig. 3 χT *vs.* T (H_{dc} = 0.1 T) and M *vs.* H (inset) plots of complex **1a**.

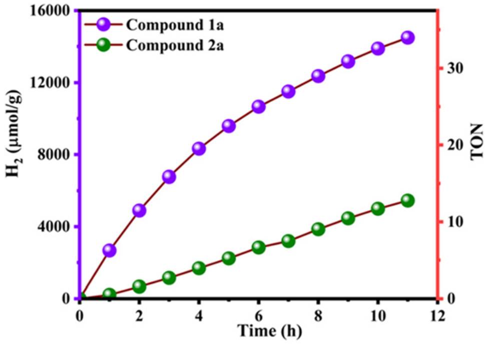

Fig. 4 Photocatalytic H_2 evolution of **1a** and **2a** under identical conditions: light source (250 W Hg-lamp), catalyst (20 μM), $[Ir(dtbbpy)(ppy)_2]^+$ (0.20 mM), TEOA (0.25 M), H_2O (2 M), 6 ml of CH_3CN-DMF (v/v = 3/2), 11 h.

below which it slowly decreases to 2.2 cm^3 K mol^{-1} at 50 K and then sharply falls to 0.95 cm^3 K mol^{-1} at 2 K, due to antiferromagnetic interactions. The signature of the χT *vs.* T plot shows moderate antiferromagnetic coupling between the body-$\{V_2^{III}O_2\}$ unit and a pair of wing-V^{IV} ions. The experimental magnetization of **1a** at 2 K under 7 T was 2.61 Nβ, indicating S = 1 and 2 states [Fig. 3, inset], supported by the χT value. Previously reported $V_2^{III}V_2^{IV}$ Schiff base complexes have shown antiferromagnetic coupling within the $\{V_4O_6\}$ core, consistent with the behaviour observed in **1a.**[28]

Photocatalytic HER studies from water were conducted using a three-component system, with the photosensitizer [4,4′-bis(1,1-dimethylethyl)-2,2′-bipyridine-*N*1,*N*1′]bis[2-(2-pyridinyl-*N*)phenyl-*C*]iridium(III) hexafluorophosphate, $[Ir(dtbbpy)(ppy)_2]PF_6$ **{Ir}** (in CH_3CN/DMF), the sacrificial electron donor triethanolamine, TEOA (in water), and complex(es) **1a** or **2a** as the catalyst (in water). Controlled experiments showed the presence of all three to be necessary for efficient HER performance. Subsequently, catalyst optimization experiments gave the maximum of hydrogen evolved at a rate of 5816 μmol g^{-1} with a catalyst concentration of 20 μM [Fig. S11, ESI† illustrates the kinetics of hydrogen production under varying catalyst concentrations]. Lower yields were obtained at slightly higher and lower catalyst concentration values, *i.e.* at 25 and 15 μM, respectively. The increasing trend of HER activity up to a certain concentration, followed by a decrease, can be attributed to accelerated decomposition of the photosensitizer by the catalyst and potential catalysis side reactions.[13]

To compare the efficacy of the mixed-valence $V^{III/IV}$-complex **1a** *vs.* the homo-valent V^{III}-complex **2a**, identical photocatalytic HER studies were performed with either **1a** or **2a** as the catalyst [Fig. 4]. Up to a period of 11 h, complex **1a** exhibited higher hydrogen evolution efficiency than **2a**. After 11 h, a yield of 14 488 μmol g^{-1}, with a TON of 33, was obtained with **1a**; while **2a** yielded 5449 μmol g^{-1}, with a TON of 8, in the same time period. Thus, complex **1a** was found to be four times more efficient than **2a**. This can be attributed to the mixed-valent nature of **1a** for H^+ reduction [see ESI†] with a desired and facile electron transfer *via* reductive quenching. In our previous report,[20] we have shown that reduction of the V^{III} centre in **2a** to V^{II} is more favourable (by 47 kcal mol^{-1}) than the oxidation to V^{IV}. Thus, the HER activity of **2a** is most likely to proceed *via* oxidative quenching [Fig. 5].

To investigate the detailed HER mechanism, oxidative *vs.* reductive [Fig. 5 inset],[29] a steady state and time-resolved fluorescence measurement of the photosensitizer **{Ir}**, with increasing concentrations of catalyst and electron donor, was performed [Fig. S12(a and b), ESI† respectively]. The kinetics of the radiative deactivation pathway of the photosensitizer was thus studied in the presence of the quencher (catalyst/TEOA) [Fig. 5 and Fig. S12(c and d), ESI†], and observed by the Stern–Volmer equation

$$\frac{F_0}{F} = 1 + K_{SV}[Q] = 1 + k_q\tau[Q]$$

$$K_{SV} = k_q\tau$$

where F_0 and F are the fluorescence intensity of $\{\mathbf{Ir}\}^*$ without and with the quencher Q of concentration [Q], respectively, K_{SV} is the Stern–Volmer quenching constant, and k_q is the quenching rate constant.

The quenching rate constant (k_q) value of 1.86×10^{10} M^{-1} s^{-1} for oxidative quenching by the catalyst **1a**, and 2.87×10^7 M^{-1} s^{-1}

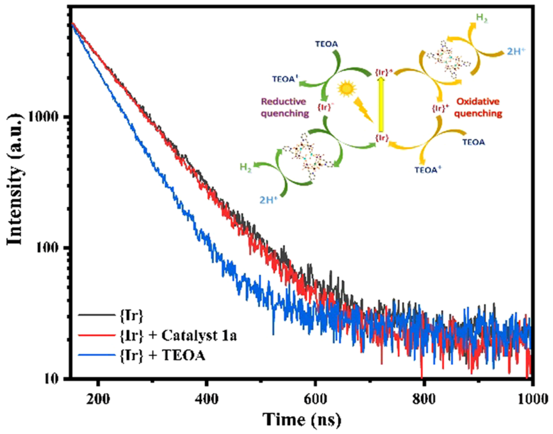

Fig. 5 Time-resolved luminescence decays of **{Ir}** (0.20 mM), **{Ir}** with POM (20 μM), and **{Ir}** with TEOA (0.25 M). The mechanistic scheme, oxidative *vs.* reductive, for the photocatalytic HER with **1a** (inset).

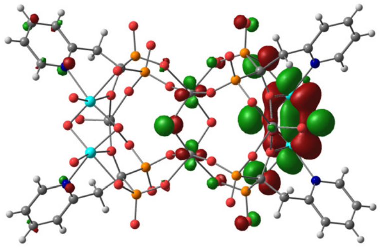

Fig. 6 SOMO of complex **1** at the B3LYP-D3(BJ)/Def2-SVP level of theory.

for reductive quenching by TEOA [Fig. S12(d), ESI†] suggests that the oxidative quenching is more dominant than reductive quenching. Fluorescence study of the photosensitizer {**Ir**} in the absence of a quencher shows a mono-exponential fluorescence decay, with a lifetime of around 86 ns [Fig. 5]. Meanwhile, in the presence of electron donor TEOA, the fluorescence lifetime of the photosensitizer {**Ir**} is reduced to 61.40 ns [Fig. S12(f) and Table S6, ESI†], representing an effective reductive quenching process. However, in the presence of the catalyst, no significant change in the lifetime of the photosensitizer {**Ir**} was observed [Fig. S12(e), ESI†]. These spectroscopic data suggest that both the catalyst and TEOA may simultaneously oxidatively and reductively quench the excited state of the photosensitizer, {**Ir**}*. However, owing to the higher concentration of TEOA and fluorescence quenching behaviour, the reductive pathway is expected to be the dominant one [**1**; $V_2^{IV}V_2^{III}$ + Ir* + TEOA → $V_2^{IV}V_2^{III}$ + Ir^- + $TEOA^+$ → $V^{IV}V_3^{III}$ + Ir + $TEOA^+$; 2 $V^{IV}V_3^{III}$ + 2 H^+ → 2 $V_2^{IV}V_2^{III}$ + H_2]. The SOMO of **1** represents the $Mo_2^{V}V^{IV}$ triangular unit, responsible for nesting one electron from Ir^- [Fig. 6]. In contrast, oxidative quenching of the Ir-complex pathway is more likely to be the dominant pathway involving **2** as an electron transfer catalyst [**2**; V^{III} + Ir* + TEOA → V^{II} + Ir^+ + TEOA → V^{II} + Ir + $TEOA^+$; 2 V^{II} + 2 H^+ → 2 V^{III} + H_2],[20] having the $(Mo_2^{VI})_2V^{III}$ unit [see ref. 20 for electronic structure of **2**].

In summary, novel diphosphonate-functionalized oxo-vanado-molybdate complexes, comprising a tetranuclear mixed valence $Mo_4^{V}V_2^{IV}V_2^{III}$ (**1**) and homo-valent $Mo_4^{VI}V^{III}$ (**2**) unit were isolated, and characterized. Spectroscopic characterization and magnetic susceptibility measurements have been carried out to confirm the mixed-valent nature of vanadium in **1**. The compounds were further shown to act as efficient electron transfer catalysts for the hydrogen evolution reaction (HER), in combination with an iridium photo-sensitizer. Comparative HER studies show that the activity of the tetra-nuclear mixed valence $V^{III/IV}$-complex (**1a**) is higher by a factor of four than that of the mono-nuclear V^{III}-complex (**2a**).[24] Quenching studies of the Ir-complex, for HER mechanistic studies, show the reductive quenching pathway for catalytic electron transfer activity to be dominant involving **1a**, while the oxidative quenching pathway is more likely employing **2a** as an electron transferring catalyst to H^+ ions.

K. S. M. and P. S. thank VNIT, Nagpur for providing a doctoral fellowship. The authors are grateful to DST-FIST (SR/FIST/CSI-279/2016(C)) for the characterization facility. The authors acknowledge SAIF IIT Patna; Prof. Fenske, Karlsruhe Nano Micro Facility (KNMF), KIT, Germany; Dr S. K. Nayak, VNIT, for SCXRD. K. C. M. thanks DST FIST for several facilities at IIT M.

Data availability

The data supporting this article (tables, figures and details of photo-catalysis) have been included as part of the ESI.† CCDC 2369137 (**1a**)† and 2442530 (**2a**)† contains the supplementary crystallographic data for this paper.

Conflicts of interest

There are no conflicts to declare.

Notes and references

1 J. J. Stracke and R. G. Finke, *ACS Catal.*, 2014, **4**, 909–933.
2 R. J. Liu and C. Streb, *Adv. Energy Mater.*, 2021, **11**, 2101120.
3 H. El Moll, *et al.*, *Inorg. Chem.*, 2012, **51**, 7921–7931.
4 G. Rousseau, *et al.*, *Chem. – Eur. J.*, 2015, **21**, 12153–12160.
5 I. Dincer and C. Acar, *Int. J. Hydrogen Energy*, 2015, **40**, 11094–11111.
6 I. Ullah, A. Munir, A. Haider, N. Ullah and I. Hussain, *Nanophotonics*, 2021, **10**, 1595–1620.
7 H. Lv, *et al.*, *Chem. Soc. Rev.*, 2012, **41**, 7572–7589.
8 X.-J. Kong, Z. Lin, Z.-M. Zhang, T. Zhang and W. Lin, *Angew. Chem., Int. Ed.*, 2016, **55**, 6411–6416.
9 J. Zhu, J. J. Walsh, A. M. Bond, T. E. Keyes and R. J. Förster, *Langmuir*, 2012, **28**, 13536–13541.
10 Z. Zhang, Q. Lin, S.-T. Zheng, X. Bu and P. Feng, *Chem. Commun.*, 2011, **47**, 3918–3920.
11 G.-H. Zhang, W.-B. Yang, W.-M. Wu, X.-Y. Wu, L. Zhang, X.-F. Kuang, S.-S. Wang and C.-Z. Lu, *J. Catal.*, 2019, **369**, 54–59.
12 T. Cui, L. Qin, F. Fu, X. Xin, H. Li, X. Fang and H. Lv, *Inorg. Chem.*, 2021, **60**, 4124–4132.
13 J. Zhao, Y. Ding, J. Wei, X. Du, Y. Yu and R. Han, *Int. J. Hydrogen Energy*, 2014, **39**, 18908–18918.
14 D. Shi, R. Zheng, C.-S. Liu, D.-M. Chen, J. Zhao and M. Du, *Inorg. Chem.*, 2019, **58**, 7229–7235.
15 G. Paille, *et al.*, *Chem. Commun.*, 2019, **55**, 4166–4169.
16 M.-P. Santoni, G. La Ganga, V. Mollica Nardo, M. Natali, F. Puntoriero, F. Scandola and S. Campagna, *J. Am. Chem. Soc.*, 2014, **136**, 8189–8192.
17 C. Streb, in *Polyoxometalate-Based Assemblies and Functional Materials*, ed. Y. F. Song, 2018, vol. 176, pp. 31–47.
18 D. Thakre, *et al.*, *Cryst. Growth Des.*, 2021, **21**, 4285–4298.
19 K. S. Morla, T. B. Deshmukh, R. K. Aparna, B. R. Sankapal and A. Banerjee, *Energy Fuels*, 2024, **38**, 21482–21497.
20 K. S. Morla, *et al.*, *J. Mater. Chem. A*, 2024, **12**, 22013–22029.
21 D. Thakre, PhD thesis, Visvesvaraya National Institute of Technology, 2022, **https://hdl.handle.net/10603/441989**.
22 X. Luo, F. Wu, H. Xiao, H. Guo, Y. Liu and S. Tan, *Synth. Met.*, 2017, **223**, 205–211.
23 C. Wu, J. Tong, J. Gao, J. Li, X. Li, J. Zhu, M. Gu and W. J. A. A. E. M. Zhou, *ACS Appl. Energy Mater.*, 2021, **4**, 1120–1129.
24 G. Silversmit, *et al.*, *J. Electron Spectrosc. Relat. Phenom.*, 2004, **135**, 167–175.
25 M. C. Biesinger, *et al.*, *Appl. Surf. Sci.*, 2011, **257**, 2717–2730.
26 J. Krzystek, A. Ozarowski, J. Telser and D. C. Crans, *Coord. Chem. Rev.*, 2015, **301–302**, 123–133.
27 M. A. Augustyniak-Jablokow, S. A. Borshch, C. Daniel, H. Hartl and Y. V. Yablokov, *New J. Chem.*, 2005, **29**, 1064–1071.
28 I. S. Tidmarsh, *et al.*, *Inorg. Chem.*, 2007, **46**, 9743–9753.
29 G. Paille, *et al.*, *Chem. Commun.*, 2019, **55**, 4166–4169.